International Journal of Engineering Research and Technology. ISSN 0974-3154, Volume 12, Number 10 (2019), pp. 1769-1777

Evaporation Estimation of a Temporary Pond in Arid Region Using Aerodynamic, Combined, and Energy Balance Models

Azel Almutairi[1*]
[1]Kuwait University, Environmental Technology Management Department, 13060, Safat, Kuwait.
**Corresponding author: azel.almutairi@ku.edu.kw, ORCID: 0000-0003-3104-8042*

Abstract:

Measuring the evaporation rate from water bodies is crucial. In this study, on-site measurements were performed, and it was incorporated with the evaporation rate modeling. Three different mechanisms.; namely, aerodynamic modeling, energy balance modeling, and combination modeling were adopted for evaporation determination of a temporary pond in an arid environment, in Kuwait. The meteorological data was obtained from the Department of Meteorology, Directorate General of Civil Aviation, Kuwait, the airport station, and statistical tests were conducted to investigate the selected models' performance. The energy balance models showed significant agreement using the Bland and Altman analysis, and the Dalton, Holman, and Harbeck models gave the lowest RSME and MBE values of 0.113, 0.061, 0.133 and 0.028, 0.23, -0.035 respectively. The derived Energy Balance model gave the optimum regression line of 1.0665x + 0.0789 with R^2 equal to 0.7804.

Keyword: Evaporation, Energy balance, Aerodynamic models, Mass transfer.

NOMENCLATURE:

All the following paraments have the specified units unless mentioned in the text otherwise.

E_P	Evaporation rate from the water body, $\frac{mm}{day}$
N_m	Mass transfer coefficient, $\frac{m}{s}$, or $\frac{mm.s}{m.kPa}$
u	Wind speed measured at 2 m over the water, $\frac{m}{s}$
e_s	Saturation vapor pressure, kPa
e_a	Vapor pressure, kPa
Q_{evap}	Evaporation Heat Flux, $\frac{W}{m^2}$
ρ_w	Water density, $\frac{kg}{m^3}$
h_{fg}	Latent heat of vaporization, $\frac{J}{kg}$
A_s	area of the water surface, m^2
Δ	slope of saturation vapor pressure and temperature at temperature T, $\frac{de}{dT}$, $\frac{kPa}{℃}$
γ	Psychometric parameter, $\frac{kPa}{℃}$
E_{ap}	Aerodynamic part in Penman model, $\frac{mm}{day}$
P	Atmospheric pressure, kPa
c_{pa}	Specific heat of moist air, $\frac{kJ}{kg℃}$
c_{pw}	Specific heat of water, $\frac{kJ}{kg℃}$
ϵ	Ratio of the molecular weight of water vapor to that of dry air
Z	Elevation of the site, m
T_s	Surface temperature of the water, °C
R_n	Daily average net radiation, $\frac{mm}{day}$
S_n	Daily average net solar radiation, $\frac{mm}{day}$
L_n	Daily average net longwave radiation, $\frac{mm}{day}$
f	Cloud factor
T_{air}	Daily average air temperature in equation (14), K
ε'	effective emissivity
S^d	Daily total solar radiation, $\frac{mm}{day}$
S^d_{clear}	Daily total solar radiation for clear sky, $\frac{mm}{day}$
a_s, b_s	Empirical constants of equation (16)
n	Bright sunshine hours, hours
N	Day lasting hours, hours
a	The albedo
S^d_o	Solar constant, $\frac{mm}{day}$
d_r	Eccentricity factor
ω_s	Sunset hour angle, radians
φ	Site latitude
δ	Solar declination, radians
D_y	The day of the year (Julian Day)
ε	Water emissivity
T_{dew}	Dew-point temperature, °C
l	Conduction zone thickness, m
T_w	Bulk water temperature, K
T_s	Water surface temperature, K
G	Lake storage heat flux, $\frac{W}{m^2}$
H	Sensible heat flux, $\frac{W}{m^2}$

1. INTRODUCTION

The lack of water, especially in arid and semiarid regions, is a primary cause of desertification which has a dramatic impact on the living environment [1]. One of the main elements that enhance scarcity of water is evaporation, notably in limited water bodies such as temporary ponds. The first attempt to estimate the evaporation rate goes back to the 18th century with the Dalton's work [2] which was based on the bulk mass transfer theory. Since then, modifications to his findings were carried out by many researchers forming a class of evaporation models known as the aerodynamic models in which the evaporation process is a dynamic process occurs at the air-water interface, and hence, ambiguity occurs due to the simultaneous heat and mass transfer occurrence [3]. As a result, another class of evaporation modeling was developed to address this phenomenon which are known as energy balance (budget) models which include the basic types of heat transfer mechanisms such as conduction, convection, radiation, and evaporation. As an attempt to combine both types of models, Penman in 1948 [4] introduced a combined model that linked the mass transfer and heat transfer approaches.

The mass transfer method is an attractive method due its utilization of the data that are easily measured [5] including the meteorological variables such as wind speed, relative humidity, air temperature, and water body's surface temperature. However, defining the wind function was always a difficulty that reduces the accuracy of this approach. Lake Hefner, Holman, Harbeck, and Dalton models are very well-known models that were derived from the mass transfer theory. The energy balance method is more difficult in use compared to mass transfer method because of the difficulty of evaluation of certain terms like atmospheric radiation, reflected atmospheric radiation, reflected solar radiation, long-wave radiation from the body of water, energy conducted to or from the body of water, advected energy, and the change of energy storage in the water body. To overcome these difficulties in evaluating these terms, Penman introduced a combination model based on the mass transfer and the energy balance theories. The probable error associated with evaporation rate estimated using the Penman model with monthly data is about 8% [6]. Sacks et al [7] tested the agreement between the energy balance evaporation and mass transfer evaporation for a shallow (average 3 m in depth) and a deep lake (average 9 m in depth), and they found an error of 8 % and 24 % for the shallow and the deep lake respectively. Estimating the evaporation rate of temporarily ponds in arid and semi-arid environments is crucial for beneficial uses or recharging the groundwater [8][9][10][11]. The aim of this study is to test the three categories of the evaporation models on a temporary pond in Kuwait.

2. MATERIALS AND METHODS

2.1 Experimental Site Description

The pond is located at 29° 15′ 27′′ N and 47° 51′ 38′′ E, which is a hot desert arid climate zone. This climate is characterized by its long summer and short winter. During Summer, temperatures are usually high, while in winter weather is dry. The average annual rainfall of this region is 175 mm, and the mean annual maximum and minimum temperature are 45 °C and 28 °C in summer and 35 °C and 14 °C in winter. The pond's area is 65530 m^2 and its premises is 1092 m. Figure 1 shows the pond's location that under study.

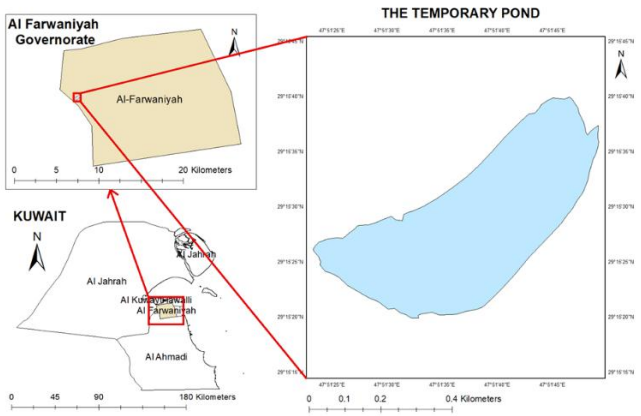

Figure 1. The pond's location on the map.

2.2. On-Site Measurements

The aerodynamic variables considered in this study were wind speed, air temperature, relative humidity, dew point temperature, wet bulb temperature, water body temperature, and the surface water (skin) temperature. Wind speed, air temperature, dew point temperature, wet bulb temperature and relative humidity were measured with a multifunctional digital anemometer (Mastech, model: MS6252B). The water surface temperature was measured with an infrared meter (Digital Instruments). The water body temperature was measured with a thermometer in a depth of 5 to 10 cm. Distance and areas were measured with a laser meter (Lecia, model: DISTOTMD1).

2.3 Meteorological Data

The meteorological data was acquired from the Department of Meteorology, Directorate General of Civil Aviation, Kuwait, the airport station. The obtained meteorology data includes wind speed, evaporation from Class A pan, bright sunshine hours, air temperature, relative humidity, and precipitation, from September 1st, 2018 to March 31st, 2019. All parameters were recorded and obtained in hourly basis.

3. EVAPORATION MODELS ANALYSIS

In this study, three categories of models will be examined; namely, the aerodynamic models, the energy balance models, and the combination models. The following analysis shows the selected models.

3.1 Aerodynamic Models

The aerodynamic models are equations that derived by the mass transfer theory, and in general it has the following form:

$$E_p = N_m f(u)(e_s - e_a) \quad (1)$$

Where the f(u) is the wind speed function. To get the

evaporation heat flux, Q_{evap}, in W/m^2, equation 2 is used:

$$Q_{evap} = E_p \rho_w h_{fg} \quad (2)$$

where Ep in equation 2 is in m/s.

3.1.1 Hefner Model

The (lake) Hefner models [4] is defined as:

$$E_P = (0.42 + 0.0040\, u)(e_s - e_a) \quad (3)$$

where E_P in inch/day, u in miles/day, and the vapor pressures are in inHg.

3.1.2 Holman Model

The Homan model [5] is expressed as:

$$E_P = 0.8(0.37 + 0.0041\, u)(e_s - e_a)^{0.88} \quad (4)$$

where E_P in inch/day, u in miles/day, and the vapor pressures are in inHg.

3.1.3 Harbeck Model

Based on an extensive measurement program on lakes in the western USA, Harbeck [6] suggested an expression for the mass transfer coefficient that merged the area of the lake. The Harbeck model for lakes in the range of 50 m < $A_s^{0.5}$ < 100 km is formulated as in equation 5:

$$E_P = 2.909\, A_s^{-0.05}\, u(e_s - e_a)^{0.88} \quad (5)$$

3.1.4 Dalton Model

The Dalton model [7] has the formulation as in equation 6:

$$E_P = 0.26(1 + 0.54\, u)(e_s - e_a) \quad (6)$$

3.1.5 Mass Transfer Correlation (MTC)

In this analysis, the air is assumed to be a quiescent fluid, hence; the average heat transfer coefficient, $\bar{h}$ in $\frac{W}{m^2 \cdot K}$, can be obtained by:

$$\frac{\bar{h}L}{k} = 0.15 Ra_L^{1/3} \quad (7)$$

where L is the characteristics length of the lake in meter (= Area/Perimeter), and k is the thermal conductivity $\frac{W}{m \cdot K}$. The left-hand side of equation (7) is known as Nusselt number, and Ra_L is Rayleigh number which is defined as:

$$Ra_L = Gr_L Pr \quad (8)$$

Where, Gr_L is Grashof number, and Pr is Prandtl number:

$$Gr_L = \frac{g(\rho_s - \rho_\infty)L^3}{\rho \nu^2} \quad (9)$$

Where g is the acceleration due gravity, ν is the kinematic viscosity (m^2/s), ρ is the average density across the boundary layer (=[$\rho_s + \rho_\infty$]/2); and ρ_s (= $\rho_{water,s} + \rho_{air,s}$) and ρ_∞ (= $\rho_{water,\infty} + \rho_{air,\infty}$) are the surface and bulk densities (kg/m^3), respectively. Invoking the heat-mass transfer analogy, the average mass transfer coefficient, $\bar{h}_m$, can be obtained by:

$$\frac{\bar{h}_m L}{D_{AB}} = 0.15 Ra_{L,m}^{1/3} \quad (10)$$

the left-hand side of equation (10) is known as Sherwood number, and D_{AB} is the binary diffusion coefficient (m^2/s), and:

$$Ra_{L,m} = Gr_L Sc \quad (11)$$

where Sc is the Schmidt number (= ν/ D_{AB}). The evaporation heat flux, Q_{evap}, in W/m^2, can be obtained by:

$$Q_{evap} = h_{fg} \bar{h}_m (\rho_{water,s} - \rho_{water,\infty}) \quad (12)$$

The applicability of the heat-mass transfer analogy is tested by the following equalities:

$$\frac{Pr}{Sc} \approx 1 \quad (13)$$

$$\frac{\bar{h}}{\bar{h}_m} \approx \frac{k}{D_{AB}} \left(\frac{D_{AB}}{\alpha}\right)^{1/3} \quad (14)$$

where α is the thermal diffusivity (m^2/s).

3.2 Combination Model

3.2.1 Penman Model

Penman model combines the practical use of the aerodynamic models and the energy balance models, and it is used widely in estimation of evaporation from water bodies. Penman model [2] is expressed as:

$$E_P = \frac{\Delta}{\Delta + \gamma} R_n + \frac{\gamma}{\Delta + \gamma} E_{ap} \quad (15)$$

Δ, slope of saturation vapor pressure and temperature at temperature, can be estimated by:

$$\Delta = \frac{4098 e_s}{(237.3 + T)^2} \quad (16)$$

γ, psychometric parameter, is determined by:

$$\gamma = \frac{c_p P}{\epsilon h_{fg}} \times 10^{-3} \quad (17)$$

the atmospheric pressure, kPa, can adjusted for the elevation of the lake, Z, as:

$$P = 101.3 \left(\frac{293 - 0.0065Z}{293}\right)^{5.256} \quad (18)$$

while the hate of vaporization, MJ/kg, can be estimated from:

$$h_{fg} = 3.501 - 0.002361 T_s \quad (19)$$

the aerodynamic part, E_{ap}, is:

$$E_P = 0.26(1 + 0.536\, u)(e_s - e_a) \quad (20)$$

the daily average net radiation, R_n, is given by:

$$R_n = S_n + L_n \quad (21)$$

where the daily average net longwave radiation is:

$$L_n = -f\varepsilon'\sigma T_{air}^4 \quad (22)$$

here, σ is Stefan-Boltzmann constant = $2\times10^{-9}\ \frac{mm}{m^2K^4day}$. For arid condition, the cloud factor, *f*, is expressed as:

$$f = 1.35\left(\frac{S^d}{S^d_{clear}}\right) - 0.35 \quad (23)$$

the daily total solar radiation ratio can be determined by the following empirical formula, with a_s = 0.25 and b_s = 0.5:

$$\frac{S^d}{S^d_{clear}} = 1.35\left(\frac{a_s + [1-c]b_s}{a_s + b_s}\right) - 0.35 \quad (24)$$

where:

$$c = \frac{n}{N} \quad (25)$$

the effective emissivity, ε', is determined by:

$$\varepsilon' = 0.34 - 0.14\sqrt{e_d} \quad (26)$$

where e_d is the daily average vapor pressure in kPa. To estimate the daily average net solar energy, the following equation is used:

$$S_n = (1-a)S^d \quad (27)$$

where a, the albedo, is the integrated reflectivity of the surface for radiation incident over the frequency range 0.15 – 4.0 μm. The typical value of the albedo for open water surfaces is 0.08 (8%). The daily total solar radiation, S^d, is found by:

$$S^d = [a_s + (1-c)b_s]S^d_o \quad (28)$$

Where, S^d_o in term of equivalent depth of evaporated water, mm/day is expressed as:

$$S^d_o = 15.39d_r(\omega_s \sin\varphi \sin\delta + \cos\varphi\cos\delta\sin\omega_s) \quad (29)$$

in which;

$$d_r = 1 + 0.033\left(\frac{2\pi}{365}D_y\right) \quad (30)$$

where, the sunset hour angel, ω_s,is the angel defines the both the beginning and end of the day; and the solar declination, δ, which is the angle between the rays of the Sun and the plane of the Earth's equator, are given respectively by:

$$\omega_s = \cos^{-1}(-\tan\varphi\tan\delta) \quad (31)$$

$$\delta = 0.4093\sin\left(\frac{2\pi}{365}D_y - 1.405\right) \quad (32)$$

3.3 Energy Balance Models

3.3.1 Energy Balance Model

The energy balance model is derived as in [4] around the air-water interface, energy to the interface is equal energy from the interface, is expressed as:

$$\alpha_s Q_{solar} + \varepsilon Q_{sky} + Q_{cond} = Q_{conv} + Q_{evap} + Q_{water} + Q_{advected} \quad (33)$$

where, Q_{solar} is the incoming solar radiation (both direct and diffuse), Q_{sky} is the radiant energy from the sky, Q_{cond} is the energy received from the water by conduction, Q_{conv} is the convective energy to/from the air, Q_{evap} is the evaporation from the water to the air, Q_{water} is the radiation energy emitted by water back to the atmosphere, $Q_{advected}$ is the energy loss due to the air bulk motion. The water emissivity, ε, and absorptivity, α, are taken to be equal since the sky temperatures is not significantly different than the water surface temperature. All *Q*'s in W/m^2. Using equation (23), Q_{evap} can be determined. $\alpha_s Q_{solar}$ can be assumed to be equal the daily average net solar energy, S^d. . The term εQ_{sky} is estimated as [13]:

$$\varepsilon Q_{sky} = (0.0727 + 0.006T_{dew})\sigma T_{air}^4 \quad (34)$$

here, σ is Stefan-Boltzmann constant, $5.67\times10^{-8}\ \frac{W}{m^2K^4}$. The heat conduction is given by:

$$Q_{cond} = \frac{k(T_w - T_s)}{l} \quad (35)$$

Q_{conv} is given by:

$$Q_{conv} = (5.7 + 3.8u)(T_s - T_{air}) \quad (36)$$

and, Q_{water} can be computed from Stephen-Boltzmann fourth-power radiation law as:

$$Q_{water} = 0.97\sigma(T_s - T_{absolute}) \quad (37)$$

Where $T_{absolute}$ is the absolute temperature of 0 °C which is equal to 273.15 K. $Q_{advected}$ is given by:

$$Q_{advected} = 0.00077(0.37 + 0.22u)\,(e_s - e_a)^{0.88}(T_s - T_{absolute}) \quad (38)$$

3.3.2 Energy Budget Model

The energy budget model is a model based on energy balance on a specified sample volume, and it takes the following form [16]:

$$R_n - G = \varepsilon\sigma T_s^4 + H + Q_{evap} \quad (39)$$

R_n here is in W/m^2. The lake storage heat flux, G, is computed from [17]:

$$G = c_{pw}\rho_w Z\frac{\partial T_w}{\partial t} \quad (40)$$

Where Z is the average depth of the lake, m, and $\frac{\partial T_w}{\partial t}$ is the

time rate change of water bulk temperature. The sensible heat flux, *H*, which is a function a of air temperature measured at 2 m, is obtained from[10]:

$$H = \rho_a c_{pa} \left[\left(\frac{\sigma_T}{0.92} \right)^3 \frac{0.82g}{T_{air} + 273.15} \right]^{1/2} \quad (41)$$

where, σ_T is the standard deviation of air temperature in °C.

3.4. Models Testing

The models performance will be examined by two statistical indicators, the root mean square error (RMSE) and mean bias error (MBE).

$$RMSE = \left[\frac{1}{n} \sum_{i=1}^{n} \left(E_{i,Model} - E_{i,Obs} \right)^2 \right]^{1/2} \quad (42)$$

and,

$$MBE = \frac{1}{n} \sum_{i=1}^{n} \left(E_{i,Model} - E_{i,Obs} \right) \quad (43)$$

Although RMSE and MBE normally provide an acceptable procedure for model performance, they do not tell whether the models' output is statistically significant or not. To test the significance of the model performance, a Student t-test will be performed; in which, the null hypothesis is assuming that the variances of the observed and the calculated evaporation rates are equal. As a result, the test statistic will be defined [19] as:

$$t = \frac{\bar{x}_1 - \bar{x}_2}{\sqrt{\frac{(n_1 - 1) \cdot s_1^2 + (n_2 - 1) \cdot s_2^2}{n_1 + n_2 - 2} \cdot \frac{n_1 + n_2}{n_1 \cdot n_2}}} \quad (44)$$

where $\bar{x}_i$, s_i^2, and n_i is the mean, variance, and the size of population *i* respectively. Here, the degree of freedom (df) is $n_1 + n_2 - 2$. Thus, the critical *t* value would be 2.1788 and – 2.1788 for a two-tailed test. The level of significance was set to be $\alpha = 0.05$.

To assess the agreement between the observed and the calculated values, the Bland and Altman plot analysis [20] will be used. The Bland and Altman analysis constructs two limits of agreement, the upper limit which equals to the mean of the two data set added to 1.96 of the standard deviation, and the lower limit which equals to the mean of the two data set subtracted from 1.96 of the standard deviation. The plot is basically an XY scatter plot, in which the Y-axis shows the difference between the two measurements and the X-axis represents the average of these measures.

4. RESULT AND DISCUSSION

4.1 On-Site Measurements

The on-site measurements of experimental variables are demonstrated on Figure 2. The air temperature, the relative humidity, and the dew point temperature readings exhibit the highest variation among the other experimental variables as shown in Figure 2. The water body temperature, the wet bulb temperature, and the surface water temperature experimental readings show a little variation comparing to the other experimental variables. This may refer to the stability conditions of water body comparing to the air metrological variables.

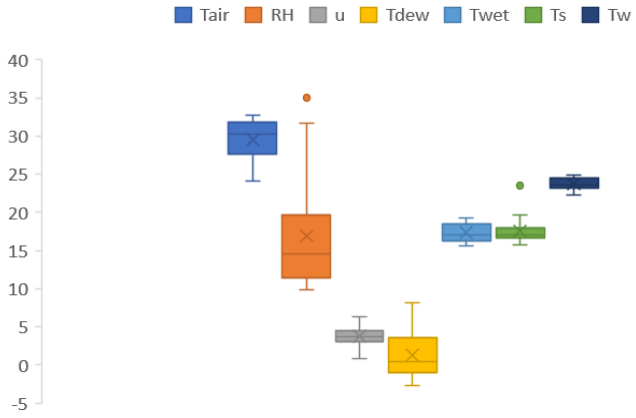

Figure 2. The on-site measurements of the experimental variables. RH is the relative humidity. The × sign referred to the mean values.

4.2 Aerodynamic Models

The aerodynamic model's evaporation rate and the evaporation flux results are shown on Figure 3 and Figure 4, respectively.

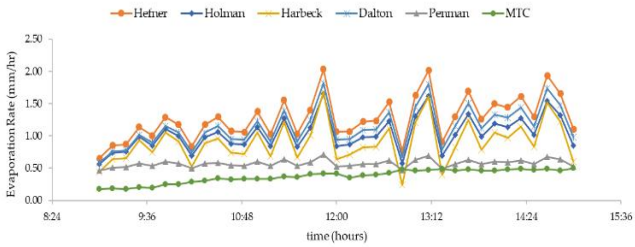

Figure 3. Aerodynamic models' estimation of evaporation rate (mm/hr).

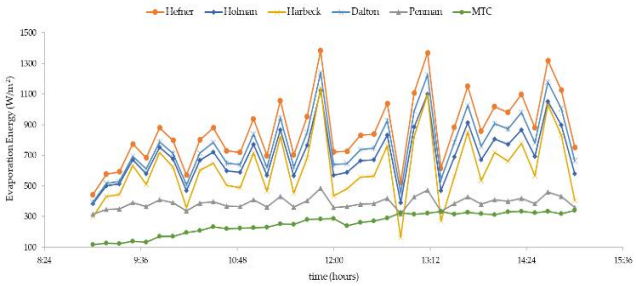

Figure 4. Aerodynamic models' estimation of evaporation flux (W/m^2).

As shown in Figure 3, the evaporation rates estimated by the aerodynamic models follow the same pattern although they are varying in magnitude. This finding may refer to the same deficit value, $\overline{D}$, (the difference between the saturated vapor pressure and the real vapor pressure) of the aerodynamic models and its

varying values of the mass transfer coefficients. This shows how the mass transfer coefficients play a critical role in estimating the evaporation rates of the aerodynamic models and thus its accuracy in this matter. In a descending order, the estimation of the evaporation flux is given by Hefner, Dalton, Holman, Harbeck, and MTC model respectively as shown in Figure 4. Since the Penman model categorized as a combined model, which has an aerodynamic part and energy balance part, it is demonstrated in Figure 3 and 4 for comparison. The main difference between the Harbeck model and the other aerodynamic models is the incorporation of the area of the water body, in this case the area of the pond. This advantage of the Harbeck model may explain why the Harbeck model is relatively closer to the Penman model. The evaporation rate and flux obtained by the mass transfer correlation (MTC) is the lowest comparing to the other models. This is an expected finding, since the quiescent assumption has been made which addresses the evaporation that due to the buoyancy variation for a still air. Indeed, the MTC model shows how the evaporation is effected by the wind motion. The applicability of the heat-mass transfer analogy, for the MTC model, is tested using equation (12) and (13), and the analogy was found applicable with Pr/Sc equals to an average of 1.003 for 37 data points.

4.3 Combined and Energy Balance Models

The combined (Penman) and energy balance model's evaporation rate and the evaporation flux results are shown on Figure 5 and Figure 6, respectively.

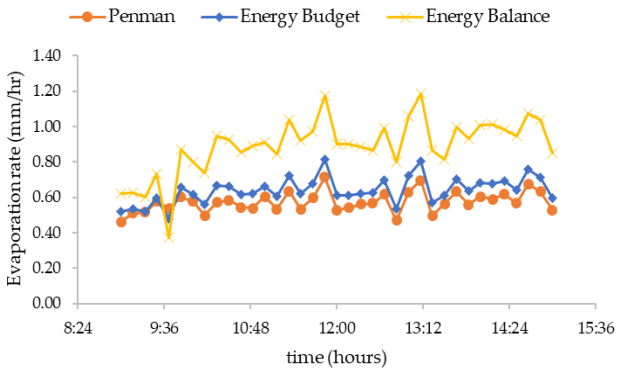

Figure 5. Combined and energy balance models' estimation of evaporation rate (mm/hr).

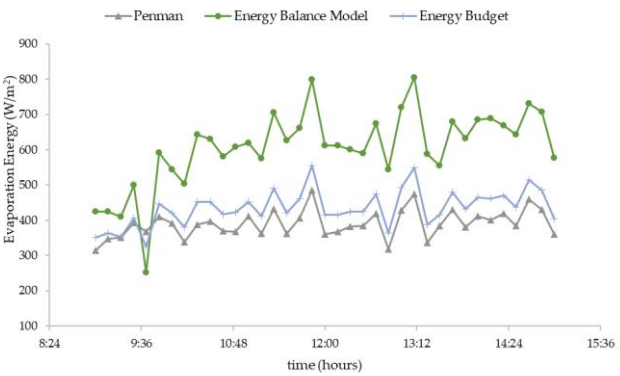

Figure 6. Combined and energy balance models' estimation of evaporation flux (W/m^2).

Although, in general, the pattern of the combined and energy balance models are similar, Figure 5 shows a clear similarity between the Penman model and the energy budget model for some intervals that are differ than the energy balance model namely, between time interval 9:20 to 9:30, 12:00 to 12:20, and 1:10 to 2:40. A possible explanation to this agreement may refer to the complexity of the energy balance model. Figure 6 shows that the energy balance model and the energy budget model gave a higher evaporating flux than the penman model. Since the aerodynamic part in Penman model contributes to nearly 50 % of the model, a comparison between the aerodynamic models and the energy balance models including the combined model is required. A comparison between all models regarding the evaporation flux is demonstrated in Figure 7. Comparing to the aerodynamic models (except for MTC model), the energy balance models and the Penman model fluctuate less. However, the MTC model is comparingly smother than all the models.

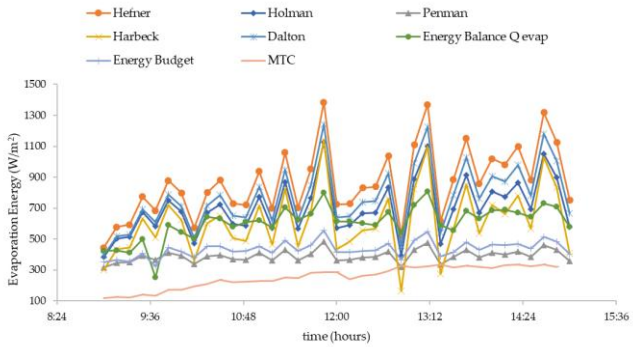

Figure 7. Evaporation flux given by all models.

To test the model's performance against the data obtained by the meteorological station, the pan evaporation rate reading was plotted along with evaporation rates obtained by the selected models in this study as shown in Figure 8.

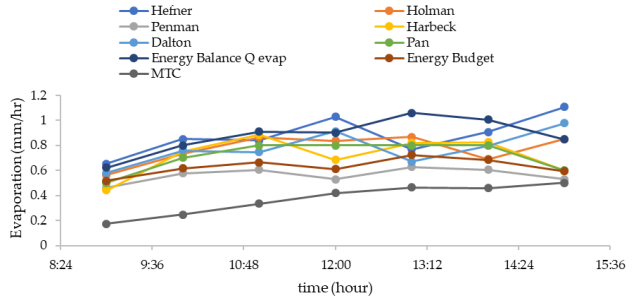

Figure 8. A comparison of the evaporation rates of the tested models in this study and the Pan (meteorological) data.

4.4 Models Testing

To test the selected models' performance to the evaporation pan meteorological data, Bland Altman plots were constructed as shown in Figure 9. In Figure 9, the solid horizontal line

represents the mean, while the dotted upper line and the dotted lower line represent the upper and lower agreements respectively.

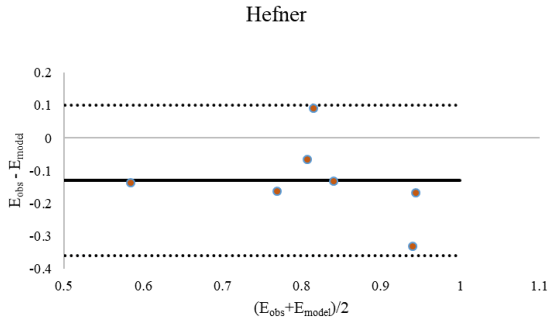

(a)

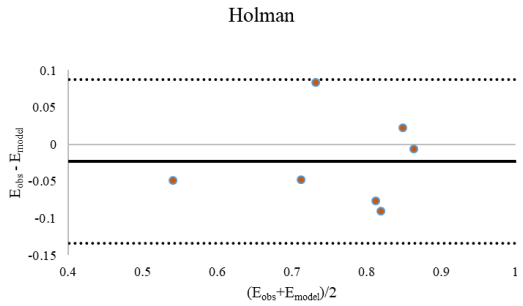

(b)

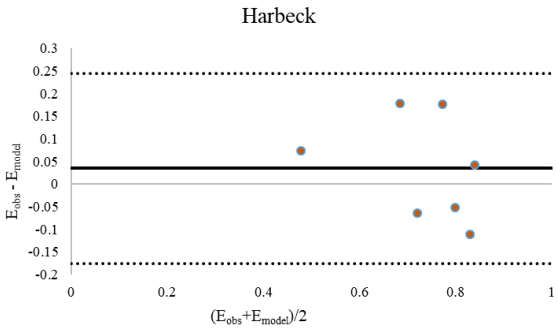

(c)

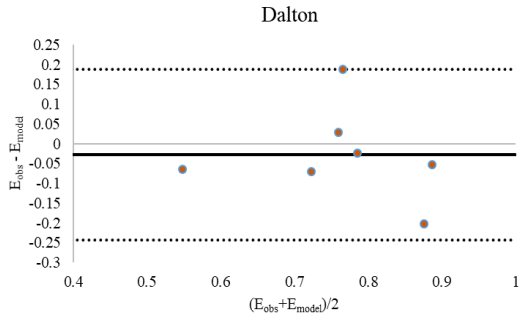

(d)

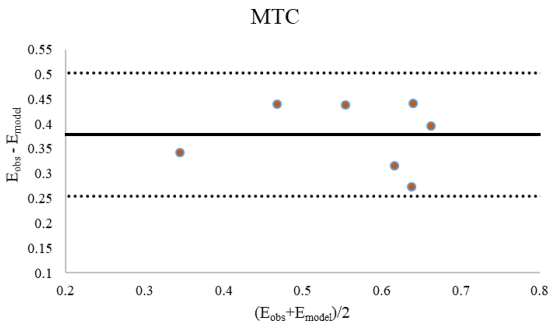

(e)

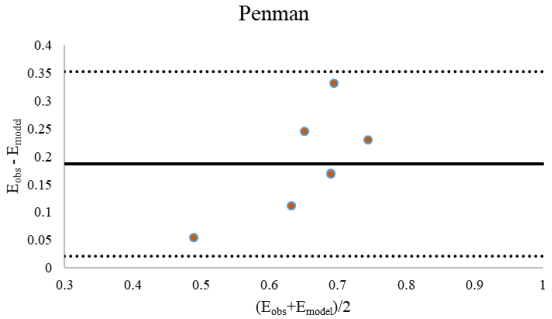

(f)

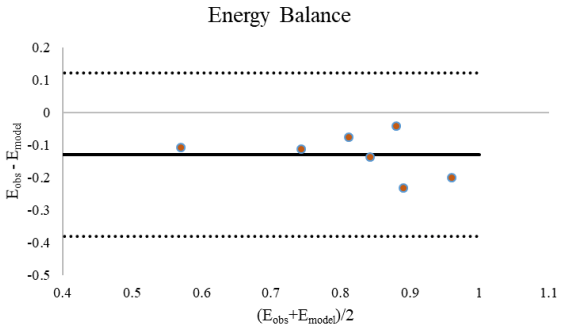

(g)

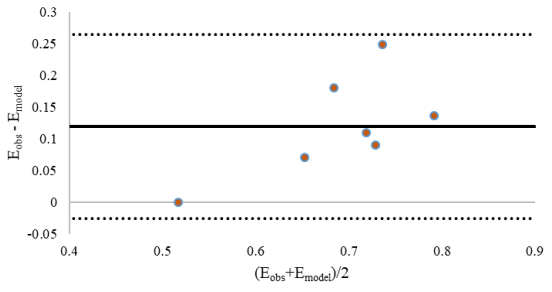

(h)

Figure 9. Bland Altman agreement plot of hourly distribution of observed meteorological evaporation rate and estimated evaporation rate of: (a) Hefner; (b) Holman; (c) Harbeck; (d) Dalton; (e) MTC; (f) Penman; (g) Energy Balance; (h) Energy Budget.

Figure 10. Bland Altman agreement plot of hourly distribution of observed meteorological evaporation rate and estimated evaporation rate of: (a) Hefner; (b) Holman; (c) Harbeck; (d) Dalton; (e) MTC; (f) Penman; (g) Energy Balance; (h) Energy Budget.

Table 1 shows the significance of the models' performance using the t-test with $\alpha = 0.05$. The models show significance performance were the models with p-value greater than 0.05, and they were in bold and italic p-value numbers on Table 1.

Table 1. The t-test matrix for the model's performance.

Model	Hefner	Holman	Harbeck	Dalton	MTC	Penman	Energy Balance	Energy Budget
Variance	0.0233	0.0131	0.0238	0.0183	0.0151	0.0034	0.0205	0.0046
Observations	7	7	7	7	7	7	7	7
df	12	12	12	12	12	12	12	12
t Stat	-1.7668	-0.3750	0.4716	-0.4105	5.8584	3.7486	-1.8294	2.3120
p-value	***0.1027***	***0.7142***	***0.6457***	***0.6887***	0.0001	0.0028	***0.0923***	0.0393
RMSE	0.174	0.061	0.113	0.113	0.384	0.206	0.143	0.140
MBE	0.129	0.023	-0.035	0.028	-0.378	-0.188	0.129	-0.119

Based on Figure 9 and Table 1, Hefner, Holman, Harbeck, Dalton, and the Energy Balance models show significance performance comparing the recorded meteorological data. For these models the p-values are greater than 0.05, hence; there are strong evidences that fail to reject the null hypothesis of equal variances, and therefore their variances are equal to the recorded meteorological evaporation rates. That means these models' outputs show significance agreements to the observed ones. As shown in Figure 9 (a-d) and (g), the plotted data points are clustered around the mean values, as a result, showing reasonable agreements. While for MTC, Penman, and Energy budget models which represented in Figure 9 (e-f) and (g), the plotted data points are relatively drifting away from the mean value (the solid horizontal line). As discussed by several studies, correlation (r or R^2) is not generally a sufficient parameter for a tested model agreement, however, correlation can give an emphasis on the observed to calculated values relationship. Therefore, regressions of the models that show significance relationship were found and shown on Figure 10.

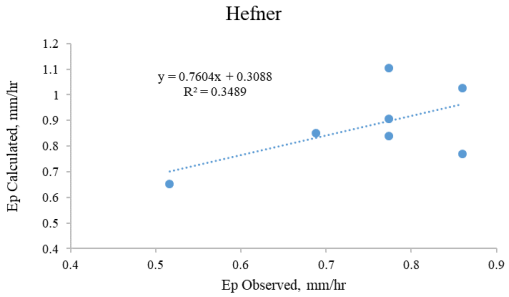

(a)

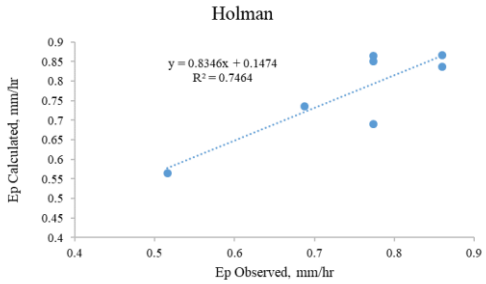

(b)

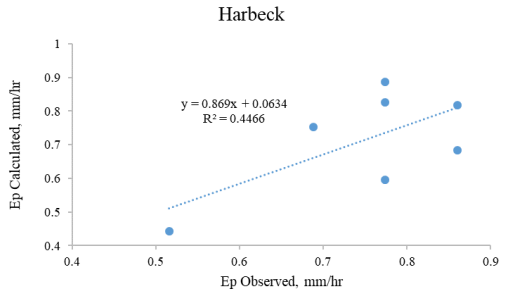

(c)

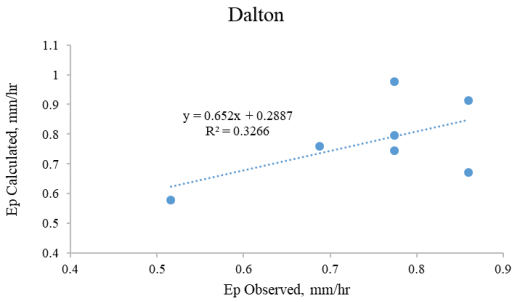

(d)

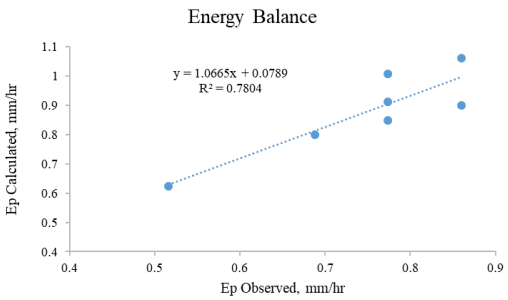

(e)

Figure 10. Correlations of the significant models prediction.

To use the regression line as an indication for agreement, the slope in the regression line plays an essential role. As the slope approaches unity, as good the model agreed with the observed values. The optimum regression line is the one with slope ≅ 1 and intercept ≅ 0. In this context, Figure 10 (e), the Energy Balance model shows the best regression line, and thus; it is the best model for the meteorological data prediction. In light of regression analysis, the models that follow the Energy Balance model with prediction of the recorded data in descending order are: Harbeck, Holman, Hefner, and Dalton model.

The RMSE and MBE are basically representing the mean difference between the observed and the predicted values. In this context, the lower the RMSE and MBE magnitude values are, the better the model is. However, since the RMSE and MBE are mean differences, they are highly affected by any large difference values, and as a result they are blind towards the under and overestimation readings. As Table 1 shows, Holman, Dalton, and Harbeck models have the lowest RMSE and MBE measures. The Energy Balance and the Budget Models have smaller RMSE and MBE values than the Penman Model.

5. CONCLUSION

Several evaporation models have been tested including aerodynamic models, energy balance models, and Penman model as a combined model. The performances of the aerodynamic models are accepted, while the energy balance models (the Energy Balance and the Budget models) show more significant performance when applied to a temporary pond in arid environment.

REFERENCE

[1] H. Meddi, M. Meddi, and A. A. Assani, "Study of Drought in Seven Algerian Plains," *Arab. J. Sci. Eng.*, vol. 39, no. 1, pp. 339–359, Jan. 2014.

[2] J. Dalton, "Experimental essays on the constitution of mixed gases on the force of steam or vapour from water and other liquids in different temperatures, both in a Torricellian vacuum and in air on," *Mem. Lit. Philos. Soc. Manchester.*, 1802.

[3] S. S. Eslamian, S. A. Gohari, M. J. Zareian, and A. Firoozfar, "Estimating Penman–Monteith Reference Evapotranspiration Using Artificial Neural Networks and Genetic Algorithm: A Case Study," *Arab. J. Sci. Eng.*, vol. 37, no. 4, pp. 935–944, Jun. 2012.

[4] H. L. PENMAN, "Natural evaporation from open water, bare soil and grass," *Proc. R. Soc. Lond. A. Math. Phys. Sci.*, vol. 139, no. 1032, pp. 120–145, 1948.

[5] V. P. SINGH and C.-Y. XU, "Evaluation and Generalization of 13 Mass-Transfer Equations for Determining Free Water Evaporation," *Hydrol. Process.*, vol. 11, no. 3, pp. 311–323, Mar. 1997.

[6] E. T. Linacre, "Data-sparse estimation of lake evaporation, using a simplified Penman equation," *Agric. For. Meteorol.*, vol. 64, no. 3–4, pp. 237–256, May 1993.

[7] L. A. Sacks, T. M. Lee, and M. J. Radell, "Comparison of energy-budget evaporation losses from two morphometrically different Florida seepage lakes," *J. Hydrol.*, vol. 156, no. 1–4, pp. 311–334, Apr. 1994.

[8] H. Haider, A. R. Ghumman, I. S. Al-Salamah, Y. Ghazaw, and R. H. Abdel-Maguid, "Sustainability Evaluation of Rainwater Harvesting-Based Flood Risk Management Strategies: A Multilevel Decision-Making Framework for Arid Environments," *Arab. J. Sci. Eng.*, pp. 1–24, Apr. 2019.

[9] H. Q. Yasin and R. S. Clemente, "Application of SWAT Model for Hydrologic and Water Quality Modeling in Thachin River Basin, Thailand," *Arab. J. Sci. Eng.*, vol. 39, no. 3, pp. 1671–1684, Mar. 2014.

[10] A. H. Azhar, M. Masood, G. Nabi, and M. Basharat, "Performance Evaluation of Reference Evapotranspiration Equations Under Semiarid Pakistani Conditions," *Arab. J. Sci. Eng.*, vol. 39, no. 7, pp. 5509–5520, Jul. 2014.

[11] I. Ladlani, L. Houichi, L. Djemili, S. Heddam, and K. Belouz, "Estimation of Daily Reference Evapotranspiration (ET0) in the North of Algeria Using Adaptive Neuro-Fuzzy Inference System (ANFIS) and Multiple Linear Regression (MLR) Models: A Comparative Study," *Arab. J. Sci. Eng.*, vol. 39, no. 8, pp. 5959–5969, Aug. 2014.

[12] Geological Survey, *Water-Loss Investigations: Lake Hefner Studies, Technical Report*. 1954.

[13] R. Eluripati, "An Improved Model for Estimating Evaporation over Lakes and Ponds," *Univ. New Orleans Theses Diss.*, Aug. 2007.

[14] G. Harbeck, "A practical Field Technique For Measuring Reservoir Evaporation utilizing Mass-Transfer Theory," *US Geol. Surv. Prof. Pap.*, vol. 272-E, pp. 101–105, 1962.

[15] *Evaporation into the Atmosphere*, vol. 9, no. 24. 2015.

[16] J. Xu, S. Haginoya, K. Saito, and K. Motoya, "Surface heat balance and pan evaporation trends in Eastern Asia in the period 1971-2000," *Hydrol. Process.*, vol. 19, no. 11, pp. 2161–2186, 2005.

[17] S. Yu, J. Liu, J. Xu, and H. Wang, "Evaporation and energy balance estimates over a large inland lake in the Evaporation and energy balance estimates over a large inland lake in the Tibet-Himalaya," no. May 2015, 2011.

[18] D. Maidment, "Handbook of Hydrology." McGraw-Hill, New York, 1993.

[19] G. Woodbury, *An introduction to statistics*. Duxbury, 2002.

[20] J. M. Bland and D. G. Altman, "Statistical methods for assessing agreement between two methods of clinical measurement.," *Lancet (London, England)*, vol. 1, no. 8476, pp. 307–10, Feb. 1986.